Analyst

PAPER

Cite this: *Analyst*, 2014, **139**, 5945

Metabolic transformation of microalgae due to light acclimation and genetic modifications followed by laser ablation electrospray ionization mass spectrometry with ion mobility separation†

Sylwia A. Stopka,[a] Bindesh Shrestha,[a] Éric Maréchal,[b] Denis Falconet[b] and Akos Vertes*[a]

Metabolic profiling of various microalga species and their genetic variants, grown under varied environmental conditions, has become critical to accelerate the exploration of phytoplankton biodiversity and biology. The accumulation of valuable metabolites, such as glycerolipids, is also sought in microalgae for biotechnological applications ranging from food, feed, medicine, cosmetics to bioenergy and green chemistry. In this report we describe the direct analysis of metabolites and lipids in small cell populations of the green alga *Chlamydomonas reinhardtii*, using laser ablation electrospray ionization (LAESI) mass spectrometry (MS) coupled with ion mobility separation (IMS). These microorganisms are capable of redirecting energy storage pathways from starch to neutral lipids depending on environmental conditions and nutrient availability. Metabolite and lipid productions were monitored in wild type (WT), and genetically modified *C. reinhardtii* strains with an impaired starch pathway. Lipids, such as triacylglycerols (TAG) and diacylglyceryl-*N*,*N*,*N*-trimethylhomoserine (DGTS), were monitored over time under altered light conditions. More than 200 ions related to metabolites, *e.g.*, arginine, cysteine, serine, palmitate, chlorophyll *a*, chlorophyll *b*, *etc.*, were detected. The lipid profiles at different light intensities for strains with impaired starch pathway (*Sta*1 and *Sta*6) contained 26 glycerolipids, such as DGTS, monogalactosyldiacylglycerol (MGDG) and digalactosyldiacylglycerol (DGDG), as well as 33 TAG species. Results were obtained over a 72 hour time period under high and low light conditions for the WT species and the two mutants. Our results indicate that LAESI-IMS-MS can be utilized for the rapid analysis of increased TAG production at elevated light intensities. Compared to WT, the *Sta*6 strain showed 2.5 times higher lipid production at 72 hours under high light conditions. The results demonstrate our ability to rapidly observe numerous changes in metabolite and lipid levels in microalgal population. These capabilities are expected to facilitate the exploration of genetically altered microalgal strains for biofuel production.

Received 25th July 2014
Accepted 4th September 2014

DOI: 10.1039/c4an01368a

www.rsc.org/analyst

Introduction

The green alga *Chlamydomonas reinhardtii* has been selected as a model organism of photosynthetic eukaryotes and explored in depth at the physiologic, genomic, transcriptomic, proteomic, metabolomic and cell biology levels. Sometimes referred to as the 'green yeast' because extensive collections of *C. reinhardtii* mutants have been generated, this organism has also become a model of choice for systems biology. It has been studied extensively for its photosynthetic properties, phototaxis, cell cycle, post-transcriptional gene silencing, and the rapid production of lipids and hydrogen for biofuel alternatives.[1–3]

Cellular metabolism of microalgae, including *C. reinhardtii* is distinguished with a high level of plasticity, where environmental conditions, *e.g.*, nitrogen starvation, can dramatically alter the flux of biochemical pathways and accumulation of metabolites.[4] For example, under high-light conditions photosynthesis is promoted, where light energy is harvested and CO_2 is utilized by the Calvin cycle.[5] Under low-light conditions carbon fixation occurs predominately through the tricarboxylic acid cycle.[6,7] As these organisms have a propensity for acclimation, nutrient deprivation or genetic modifications can be used for metabolic engineering to achieve, *e.g.*, increased lipid production.[8,9]

[a]*Department of Chemistry, W. M. Keck Institute for Proteomics Technology and Applications, The George Washington University, Washington, DC 20052, USA. E-mail: vertes@gwu.edu; Fax: +1-202-994-5873; Tel: +1-202-994-2717*

[b]*Laboratoire de Physiologie Cellulaire et Végétale, UMR 5168, CEA-CNRS-INRA-Univ. Grenoble Alpes, Grenoble, France*

† Electronic supplementary information (ESI) available. See DOI: 10.1039/c4an01368a

Due to the relative scarcity of available phosphorous, *C. reinhardtii* has a low abundance of phosphatidylcholines (PC) and a strong presence of glyceroglycolipids. Because of their structural resemblance, PC lipids are replaced by diacylglyceryl-*N*,*N*,*N*-trimethylhomoserines (DGTS) in the membranes outside plastids.[10] A class of phospholipids, phosphatidylethanolamines (PE), along with DGTS are thought to be localized in the cytoplasm.[11] In other green algae, adaptation to stress conditions results in changes in the degree of saturation for DGTS species.[12] The majority of polar lipids found in *C. reinhardtii* are galactolipids, *e.g.*, monogalactosyldiacylglycerols (MGDGs) and digalactosyldiacylglycerols (DGDGs) account for 47% and 16% of the polar lipids, respectively.[13,14] These plastid lipids play vital roles in membrane stacking and stabilization of photosynthetic complexes.[15,16] Most lipids involved in energy storage in the lipid bodies belong to the class of neutral lipids, such as triacylglycerols (TAG). Change in the environmental conditions, for example, the light level or the availability of nutrients, can result in altered lipid metabolism and in some cases significant accumulation of TAG.[17,18]

Some genetically modified strains of microalgae can exhibit redirected metabolic pathways, and provide insight into cellular lipid synthesis. For example, in the *C. reinhardtii Sta*1 mutant the defective ADP-glucose pyrophosphorylase (AGPase) enzyme leads to impaired starch production, redirecting energy storage to alternative pathways, such as lipid biosynthesis.[19,20] Combining genetic modifications and environmental factors can result in further enhancement in storage lipid production.[21–23]

The response to high-light conditions can be affected by impairing the starch pathway. The starch pathway central enzyme is AGPase and it is responsible for the formation of glucosyl nucleotides from glucose-1-phosphate with ATP. By targeting its activation enzyme, 3-phosphoglyceric acid (3-PGA), the biosynthesis of starch can be suppressed. The *Sta*1 mutant has a disrupted large catalytic subunit of AGPase, and as a consequence it exhibits reduced activation by 3-PGA. This allows the mutant to retain less than ~10% of its normal starch production.[24] The *Sta*6 mutant has a disrupted small catalytic subunit of AGPase and as a result it only retains ~1% of the normal starch levels.[21]

Conventional analysis of total and neutral lipid contents used for algae relies on staining and fluorescence microscopy.[25] However, these techniques provide no information regarding the chemical structure, degree of saturation or the acyl chain length of various lipid species in algal cells. Alternative methods for the characterization of lipids in single cells, such as Raman spectroscopy,[26] provide insight into the degree of saturation but less detail about the nature of the lipids. In contrast, NMR techniques[27] can provide chemical classification of the lipids in algae (*e.g.*, TAGs *vs.* phospholipids), but they provide little structural information and are limited by sensitivity.

For more detailed analysis, the metabolic processes in the algae are initially quenched by flash freezing and/or chemical techniques, occasionally followed by derivatization,[28] solvent extraction, chromatography and mass spectrometry (MS).[29] In some cases, quantitation relies on derivatization, *e.g.*, to form fatty acid methyl esters (FAMEs) that remove some of the structural information by converting the native, intact lipid species to their corresponding FAMEs. For example, both neutral and polar lipids can produce the same FAMEs making these lipid classes indistinguishable.[30]

An alternative method for the analysis of lipid classes is high performance liquid chromatography (HPLC). Combining HPLC with MS provides increased selectivity, resulting in a large number of separated molecular species. However high-throughput analysis is limited due to the lengthy sample preparation requirement, ranging from 2 to 4 h, and HPLC runs with typical run times of 15–40 min.[31–34] These techniques alone or in combination have been used for the detection of lipids in *C. reinhardtii* in altered environments, *e.g.*, in nitrogen or sulphur deprivation.[34,35]

Other MS based lipidomics methods include electrospray ionization MS,[36,37] matrix assisted laser desorption ionization (MALDI),[38] and desorption electrospray ionization mass spectrometry (DESI-MS).[39] In saltwater microalgae under diverse culture conditions, several lipid classes including glycerolipids, phospholipids, and neutral lipids were observed by MALDI-MS.[40] The detection of natural products and metabolites on the surface of marine algae was observed by DESI-MS. Laser ablation electrospray ionization (LAESI) utilizes mid-infrared laser pulses for the ablation of water containing samples followed by electrospray ionization.[41,42] The deposition of laser energy in samples with high-water content is enabled by the strong absorption maximum of water at 2.94 μm wavelength. Ambient ionization methods, including DESI and LAESI, require reduced time for sample preparation, typically less than 5 min, and preserve molecular information during analysis.

Ion mobility separation (IMS) techniques have been utilized in areas such as environmental sciences, drug development, and homeland security.[43–45] There is growing interest in using the combination of IMS and MS for additional selectivity for the separation and detection of structural isomers, isobars, and conformers. Differentiation of chemical species with identical *m*/*z* by IMS is based on their differences in collision cross-sections defined by sizes and shapes.[46–49] Depending on these properties, in IMS ions with identical *m*/*z* different drift times (DT) are produced and can be distinguished. Applications of IMS-MS are found in various fields of biology, including the analysis of protein complexes[50] and metabolic profiling of bacteria.[51] Recent developments in coupling IMS with LAESI-MS have been used for the increase in molecular coverage for high-throughput cell and tissue analysis.[52] Lipidomic analysis with IMS-MS has been used for the classification of lipid species, to locate position of acyl chains, and to identify double bond sites.[53–55]

In this study, we utilized IMS-MS retrofitted with a LAESI ion source for time profiling metabolites and lipids in wild type and genetically modified *C. reinhardtii* under varied light conditions. High-throughput speciation and structural identification of lipids were achieved by LAESI-IMS-MS.

Experimental

Cell culture and growth conditions

Wild type *C. reinhardtii* (CC125) and the *Sta*1 (CC4325) and *Sta*6 (CC4567) mutants were purchased from the Chlamydomonas

Resource Center at the University of Minnesota. Cell cultures were inoculated in tris acetate phosphate medium (Life Technologies, Carlsbad, CA) and maintained at 27 °C in an orbital shaker incubator (MaxQ400, Thermo Scientific, Waltham, MA) at a constant rate of 80 rpm. These cultures were illuminated with LED light bulbs (daylight white, 6 and 10 W) installed above the flasks with a photosynthetically active radiation (PAR) of 100 μmol m^{-2} s^{-1} measured using a PAR meter (Sun System, Sunlight Supply Inc, Vancouver, WA). Prior to light treatment, starting cell cultures were ~10^3 cells per mL and were acclimated for 2 cell generations (48 h) in a 12 h/12 h light/dark cycle. Light treatment consisted of two conditions, high light (HL) (150 μmol m^{-2} s^{-1}) provided by two LED sources (daylight white, 13 W) and low light by covering the culture flasks with aluminium foil (LL) (0 μmol m^{-2} s^{-1}). Cell concentrations were measured with a hemacytometer (Bright-Line, Horsham, PA) with final concentrations reaching ~10^6 cells per mL. Metabolite measurements were taken at 0, 24, 48 and 72 h after light exposure.

Sample preparation

Final cell suspensions were centrifuged for 1 minute at 5000 × *g* to produce a cell pellet. The supernatant was removed leaving a cell pellet of ~40 μL. The cell pellet was then filtered through an EconoSpin silica membrane (1 μm pore size) spin tube (Epoch Biolabs, Missouri City, TX) for 1 minute at 2000 × *g*, removing any remaining supernatant. To validate cell viability after both spin processes, cells were removed from the silica filter and resuspended in tris acetate phosphate medium. Cells were cultured and monitored over a 48 h time period and showed similar growth rates as prior to spinning. The spin tube containing the cell pellet was immediately frozen in the vapour over liquid nitrogen, preventing any changes in metabolite responses. Once frozen the silica membrane containing the cell pellet was removed from the spin tube and deposited onto a Peltier stage for LAESI-IMS-MS analysis. This method eliminated the need for a washing protocol that can induce osmotic shock and alter the metabolic state. Overall, the time required for sample preparation was less than 5 min.

LAESI

A homebuilt LAESI ion source consisting of an optical parametric oscillator, pumped by a Nd:YAG laser, (Opolette 100, Opotek, Carlsbad, CA) with a 5 ns pulse length, 2.94 μm wavelength, and 20 Hz repetition rate was used. The laser was coupled to the frozen *C. reinhardtii* cell pellet located on the silica membrane through a 75 mm focal length ZnSe lens (Infrared Optical Products, Farmingdale, NY). A homebuilt Peltier stage maintained the cell pellet and silica membrane at a low temperature (0 °C) during ablation. The resulting ablation plume was intercepted by an electrospray from a solution composed of 50% methanol with 0.1% (v/v) acetic acid supplied by a syringe pump (Physio 22, Harvard Apparatus, Holliston, MA) at a 400 nL min^{-1} flow rate through a stainless steel emitter (MT320-50-5-5, New Objective, Woburn, MA). The emitter, positioned on-axis with the inlet orifice, was kept at a constant +3.3 kV voltage using a regulated power supply (PS350, Stanford Research Systems, Sunnyvale, CA). The ionized plume was sampled using a quadrupole time-of-flight mass spectrometer (Synapt G2S, Waters, Milford, MA) equipped with traveling-wave ion mobility separation (IMS).

Ion mobility separation

IMS experiments were performed with a traveling-wave (T-wave) system, where generated ions traversed through a periodic electric field and interacted with the inert background gas. The number of collisions is reflected by the drift time within the drift cell and correlates directly with the collision cross-section of the ion. Nitrogen, used as the drift gas, was supplied at a flow rate of 90 mL min^{-1} and a pressure of 3.35 mbar. The IMS wave velocity and height were kept constant at 700 m s^{-1} and 27 V, respectively. A complete LAESI-IMS-MS analysis is shown in Fig. 1.

Time-aligned parallel fragmentation

Time-aligned parallel (TAP) fragmentation provided structural information for selected ions, such as the head group classification and the acyl chain lengths for lipids. Ions were first selected and isolated using the quadrupole analyser and fragmented in the trap cell for the production of first generation ions. The fragments then entered through the helium cell with a He flow rate of 180 mL min^{-1}. This process minimized further fragmentation by reducing the internal energy. The first generation fragment ions entered the IMS cell and were separated by their DT. The separated first generation product ions then entered the transfer cell, where they further fragmented through collision induced dissociation (CID) into time-aligned second generation fragments.

In the trap cell, the wave velocity and height were maintained at 60 m s^{-1} and 10 V, respectively, whereas in the transfer cell the wave velocity and height were kept constant at 191 m s^{-1} and 0.1 V, respectively. Both CID cells used argon as the collision gas with a flow rate of 2 mL min^{-1}. Fragmentation *via* TAP

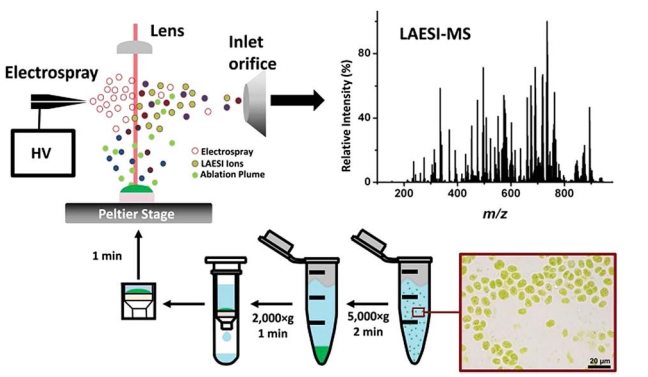

Fig. 1 Schematic representation of sample preparation of *C. reinhardtii* cells for LAESI-IMS-MS analysis. An infrared beam ablated the *C. reinhardtii* pellet off the filter disk and produced a mostly neutral plume (solid dots). Electrospray ions (open circle) aid in the generation of LAESI ions (outlined dots). The ions were separated based on their drift times and analysed by their *m*/*z* using MS.

was run in two different modes, either at a constant 30 eV energy or with energies ramped between 30 and 50 eV. The release time for the trap was 200 μs and the wave delay release was set at 450 μs.

Data processing

Tentative peak assignments were established based on accurate mass measurements, isotope distribution patterns, tandem MS measurements (assessed through the NIST 12 MS/MS Database and Search program), and TAP fragmentation patterns. Identification was enhanced through metabolite and lipid database matches in the Plant Metabolic Network (http://plantcyc.org/, last accessed on May 10, 2014) and Lipids Maps (http://lipidmaps.org, last accessed May 10, 2014) resources. For all the reported ions, *m*/*z*, drift times (DT) and intensities were determined by LAESI-IMS-MS.

To visualize these datasets, the DriftScope 2.4 module (Waters, Milford, MA) was used to produce a DT *vs.* *m*/*z* plot with the intensities presented on a false colour scale. Domains of this two-dimensional plot can be extracted to generate an enhanced mass spectrum with significantly reduced interferences (MassLynx 4.1, Waters, Milford, MA).

Results and discussion

High-throughput analysis of *C. reinhardtii*

Direct LAESI-IMS-MS analysis of *C. reinhardtii* cell pellets proved to be a robust technique for the detection of their metabolites and lipids. Incorporation of the silica membrane spin tube to separate the medium prior to analysis resulted in a significant reduction in spectral interferences and enhanced signal detection. Cellular viability, before and after silica membrane separation, was observed by bright field microscopy. Representative images of *C. reinhardtii* directly from the culture and after processing are shown in Fig. 2a. The sample preparation process, including the silica membrane separation, took less than 5 min.

Ion separation by IMS occurs within ~120 ms and the entire process of analysis required less than 150 ms. The generated DT *vs.* *m*/*z* plots were subjected to peak finding to identify the *m*/*z* and DT values of the detected species (Fig. 2b). A typical mass spectra of ~2000 cells, analysed in one second, are shown in the inset of Fig. 2b. It is dominated by over 100 lipid and lyso-lipid species in the $450 < m/z < 950$ region. With the incorporation of IMS, the number of spectral features increased approximately three folds from 170 to 470.

Signal enhancement was observed for ions of interest directly from cell samples by selecting the relevant DT. For example, in Fig. 2c, for chlorophyll *a* ions only noise was observed ($S/N < 3$) in a low cell count mass spectrum without IMS (right). With IMS at a defined DT of 160 ms, however, a substantially improved $S/N \approx 40$ enabled the detection of chlorophyll *a* ions, including the natural isotope distribution pattern (see the left panel in Fig. 2c). Comparison of the intensities of the measured isotope peaks for M + 1, M + 2 and M + 3 with the calculated intensities (see the inset in Fig. 2c) revealed 1.4%, 5.9% and 7.2% deviations, respectively. Thus, in

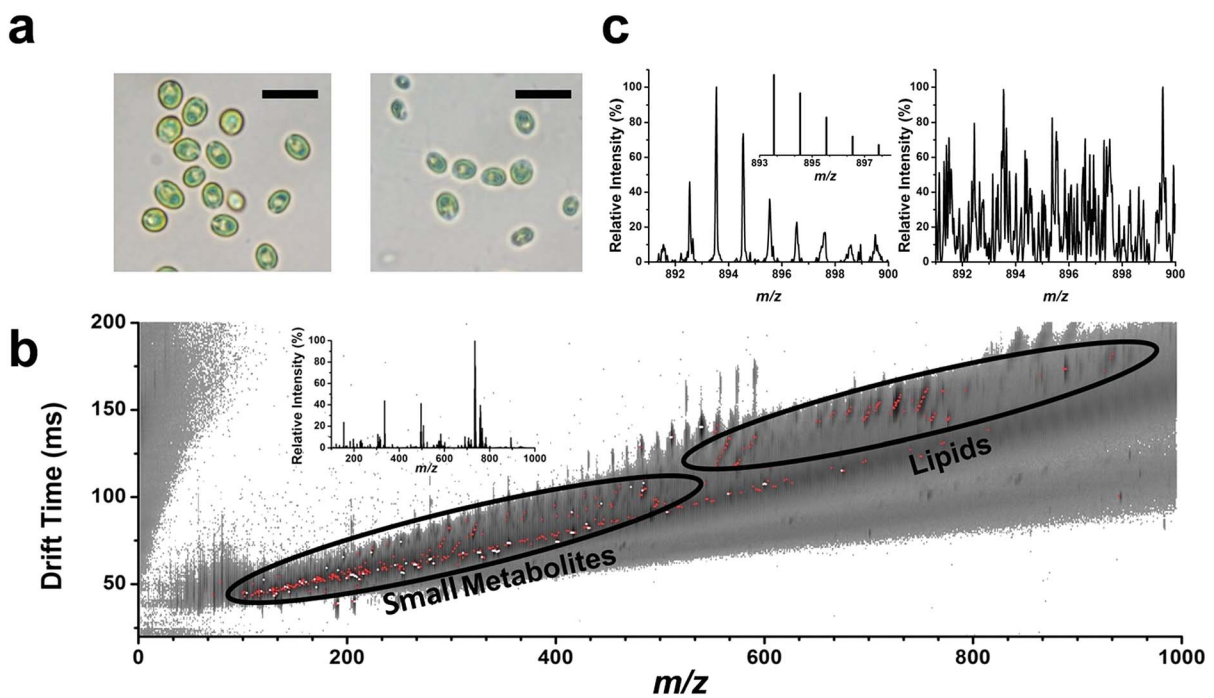

Fig. 2 (a) Representative microscopy image of *C. reinhardtii* cells before (left) and after (right) centrifugation in a spin tube (scale bar represents 20 μm). (b) Corresponding DT *vs.* *m*/*z* map with highlighted regions representing primarily small metabolites and lipids. Red dots indicate *C. reinhardtii* ions, whereas white dots indicate background ions from the electrospray. The inset shows a mass spectrum averaged over the entire drift time (DT) range. (c) The LAESI mass spectrum between *m*/*z* 890 and 900 shows no discernible peaks without IMS (right), and a clear set of isotope peaks of chlorophyll *a* for a defined DT of 160 ms with IMS (left).

a more general sense, IMS provided signal enhancement and an increased molecular coverage while maintaining high throughput.

Lipid classification and identification by LAESI-IMS-MS

The DT *vs.* *m/z* map of the lipid region in Fig. 3 showed different lipid classes, *e.g.*, DGTS, MGDG, DGDG, and TAG, separated. For lipid class identifications, characteristic fragments were generated by tandem MS from the galactosyl head group, $[C_9H_{16}O_6 + Na]^+$, observed at *m/z* 243, the digalactosyl head group, $[C_{15}H_{26}O_{11} + Na]^+$, found at *m/z* 405, and the trimethyl-serine head group, $[C_{10}H_{21}NO_5 + H]^+$, appearing at *m/z* 236.

Each family of lipids had a series of constituents, with each of them exhibiting *m/z* values increasing by two mass units, corresponding to a reduction in the degree of unsaturation. For example, the family starting with the unsaturated TAG (52 : 8) at *m/z* 864 showed a series of eight peaks with an increment of two mass units, corresponding to an increase in saturation, up to the fully saturated TAG (52 : 0) at *m/z* 880. Increasing the degree of saturation within a lipid family invariably resulted in longer drift times, *i.e.*, increased collision cross-sections.

Due to the small glycerol head group and only two acyl chains, diacyl-glycerol (DAG) lipids, the precursors of TAG, had the shortest DT. Ions with an additional acyl chain corresponded to TAG with a longer DT. Membrane lipids, such as diacylglycerolhomoserine (DGHS), DGTS, MGDG and DGDG exhibited DT values between those of the DAG and TAG species.

For additional identification of the lipid structures, time-aligned parallel fragmentation (TAP) was implemented. As shown in Fig. 4, from the DT *vs.* *m/z* map two DT ranges were selected to capture the fragmentation within the trap and transfer cells. When the DT range of 2.7–3.2 ms was selected, only the parent peak of *m/z* 734 was detected in the trap, whereas in the transfer cell both the precursor ion and a palmitic acid fragment at *m/z* 496 were detected. When the DT range of 1.5–2.0 ms was selected, the information from the trap cell contained the results from the transfer cell with 2.7 < DT < 3.2 ms settings, with an additional peak appearing at *m/z* 474 corresponding to the other acyl chain fragment.

In these experiments, the information discussed up to this point only allowed the determination of the length of acyl chains but not the nature of the head group. Further inspection of the DT 1.5–2.0 ms range in the DT *vs.* *m/z* plot from the transfer cell, revealed the presence of the trimethyl-serine head group at *m/z* 236. Therefore, TAP fragmentation allowed the classification of this lipid as DGTS (18 : 3/16 : 0), with palmitic acid and unsaturated stearic acid acyl chains.

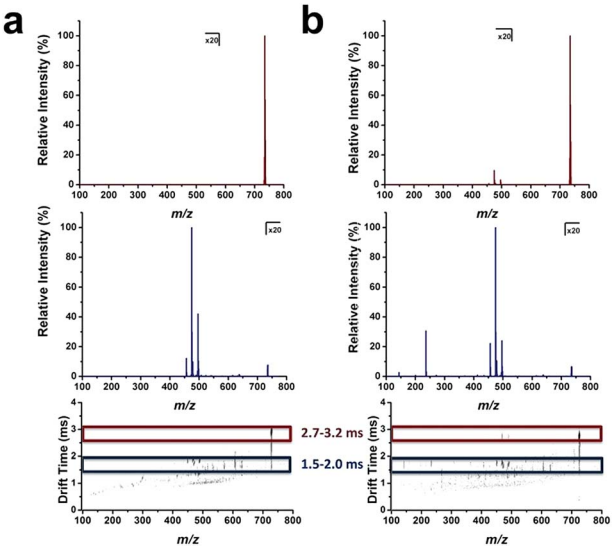

Fig. 4 (a) For tandem MS of the *m/z* 734 ion, the first generation fragment ions at DT 2.7 to 3.2 ms (top) and DT 1.5 to 2.0 ms (middle) are shown based on the DT *vs.* *m/z* map (bottom). (b) Similarly, mass spectra of the second generation ions with DT aligned fragments gave MS^3 spectra for the *m/z* 734 ion confirming its identity as DGTS (18 : 3/16 : 0).

Lipid species with two acyl chains identified in positive ion mode (seventeen DGTS, three MGDG and six DGDG) are summarized in Table S1.† DGTS lipids appeared as $[M + H]^+$ and $[M + Na]^+$, whereas MGDG and DGDG formed $[M + Na]^+$. Examples of the tandem mass spectra for the DGTS (18 : 3/16 : 0), MGDG (18 : 3/16 : 4) and DGDG (18 : 2/16 : 3) species are shown in Fig. S1–S3, respectively, of the ESI.† Table S2† lists a total of 27 neutral storage lipids, *e.g.*, TAG species, detected in positive mode as $[M + NH_4]^+$. TAG species were identified by observing neutral losses and acyl chain fragments, as well as reports of TAG with the same accurate mass in the literature. The tandem mass spectrum for TAG (52 : 7) is shown in Fig. S4 of the ESI.†

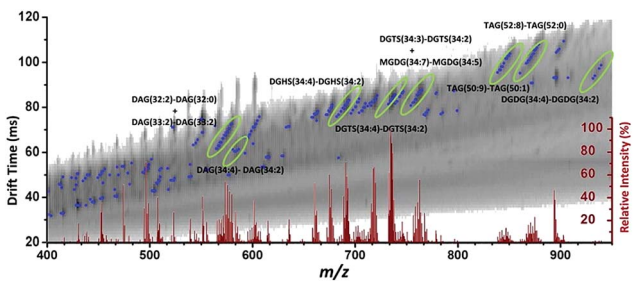

Fig. 3 DT *vs.* *m/z* map with the corresponding mass spectra for the *m/z* 400–950 range with some lipid species labelled. The map shows examples of drift time trends for lipids based on their head groups and the degree of saturation.

Metabolomic differences under light and dark conditions

To explore the metabolic effects of illumination, two cultures were raised under different light conditions. Under HL conditions, the light intensity was kept constant at 150 μmol m^{-2} s^{-1}, whereas under LL conditions the culture flasks were covered with aluminium foil. LAESI-IMS-MS was used to follow molecular changes at 0, 24, 48 and 72 hours under these two conditions (Fig. 5). As expected, at 0 h there were no significant differences between the spectra of the two cultures. With time, the metabolites and lipids in the two populations became increasingly different. Overall, lipids, *e.g.*, DGTS, MGDG, DGDG, TAG and lyso-lipids, were more abundant and diverse under HL conditions.

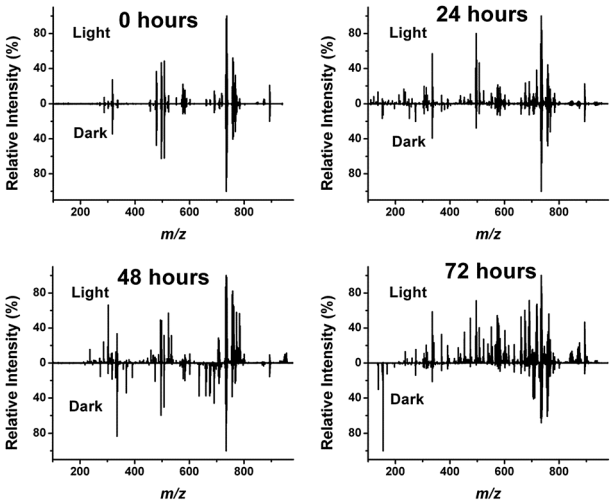

Fig. 5 LAESI-IMS-MS mass spectra of *C. reinhardtii*, cultured under HL and LL conditions for 0, 24, 48, and 72 hours, showed changes in metabolic and lipid profiles.

Kinetics of lipid production

Lipid ion intensities as a function of time under HL (150 μmol m^{-2} s^{-1}) and LL conditions were investigated for *C. reinhardtii* (Fig. 6). Members of four different lipid classes, DGTS, MGDG, DGDG, and TAG were monitored under both HL and LL conditions for over 72 hours. Initially, the cells were raised with a normal 12 : 12 h light and dark cycle under normal growth conditions. Once the HL and LL conditions were established, sampling started and was repeated every 24 h for 72 h.

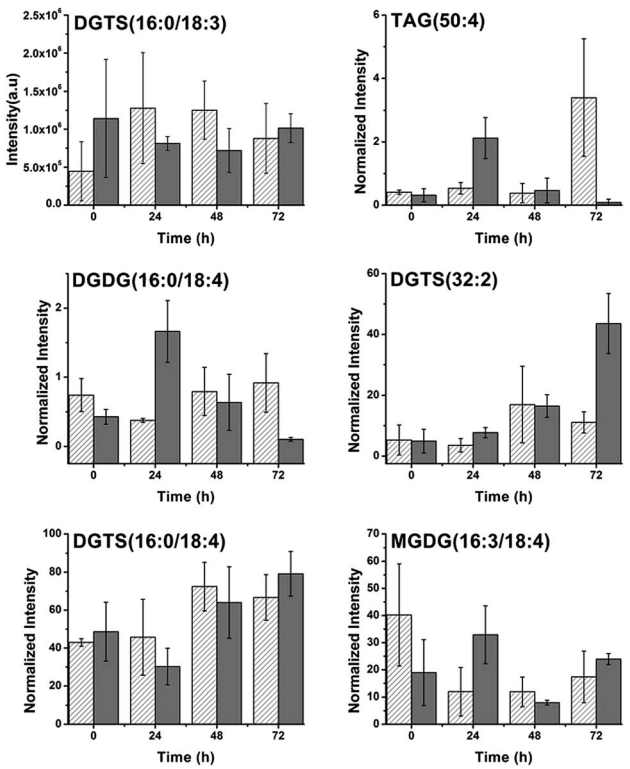

Fig. 6 Lipid ion intensities normalized to DGTS (16 : 0/18 : 3) for families of lipid species from *C. reinhardtii* as a function of time under HL (diagonal shading) and LL (grey shading) conditions.

To ascertain that lipid ion intensities could be normalized to a lipid species, DGTS (16 : 0/18 : 3), we had to verify that its ion intensity did not show significant changes over the 72 h period, and differences under HL and LL conditions were also negligible. A two-factor ANOVA test with replication indicated that $p = 0.901 > 0.05$ for time independence, meaning that with 95% significance DGTS (16 : 0/18 : 3) ion intensities did not vary in time. Similarly, for the differences between HL and LL ion intensities for this species we found that $p = 0.508 > 0.05$, meaning that the DGTS (16 : 0/18 : 3) production did not change as a function of light conditions. Based on these findings, the DGTS (16 : 0/18 : 3) intensities were used to normalize the intensities of the other lipids.

The production of TAG (50 : 4) increased eight-fold in HL during this period, whereas in LL there seemed to be a significant increase at 24 h, and then the intensity declined back to the starting level.

In contrast, the kinetics of DGDG (16 : 0/18 : 4) under HL conditions did not show significant changes throughout the observation period. In LL, there was a transient increase at 24 h, and then the peak intensities decayed back close to the starting level. Two additional DGTS lipid species were monitored, the first was DGTS (32 : 2) which under HL conditions, showed a slight increase at 48 h, and then it leveled off. Some lipid levels, *e.g.*, DGTS (16 : 0/18 : 4) and MGDG (16 : 3/18 : 4), remained essentially unchanged independent of time, ($p = 0.073 > 0.05$) and ($p = 0.244 > 0.05$), respectively, and light conditions, ($p = 0.505 > 0.05$) and ($p = 0.439 > 0.05$), respectively.

Overall, utilizing LAESI-IMS-MS revealed that the ion abundances of the TAG species, most relevant for biofuel production, showed a dramatic increase over time under HL conditions.

Storage lipid accumulation in *Sta*1 and *Sta*6 mutants

For *Sta*1 and *Sta*6 mutants, lipid abundances were followed for a total of 72 h under LL and HL light conditions, 0 and 200 μmol m^{-2} s^{-1}, respectively, and compared to the corresponding yields for the WT species. To reduce spectral interferences and differentiate isobaric species at the same nominal mass, IMS was used. For example, when a 0.4 range at the nominal *m*/*z* 894 was selected in the LAESI-IMS-MS spectrum, the DT distribution showed two distinct peaks (see the inset in Fig. 7a). The DT range integrated between 201 and 207 ms revealed the TAG (54 : 7) species at *m*/*z* 894.757, whereas between 181 and 188 ms showed the M + 1 peak of chlorophyll *a* due to the ^{13}C isotope at *m*/*z* 894.551 (Fig. 7a). This example demonstrates that without the use of IMS the two ions could not be differentiated.

Molecular coverage was greatly enhanced by the separation step. Using LAESI-MS without IMS, ~10 TAG lipid species were detected, whereas with IMS in the DT range between 189 and 204 ms the number of identified TAG increased to ~33.

Using the enhanced molecular coverage, we explored the effect of impaired starch synthesis on the production of neutral TAG storage lipids. First, the cell growth curves were compared

for the three strains to discern if the mutants exhibited altered growth. Fig. 7b shows *Sta*1 and *Sta*6 reach cell numbers comparable to the WT under HL (raised from 100 to 200 μmol m^{-2} s^{-1}) conditions. For all three strains, in LL the cell numbers were considerably lower. For *Sta*6 in LL the size of the cell population did not change significantly.

The abundances of the TAG lipids were monitored for the WT, *Sta*1 and *Sta*6 mutants over 72 h under HL and LL conditions. A total of 33 TAG-related ions between *m*/*z* 820 and 900 were integrated in the DT range of 189 to 204 ms (Fig. 7c). After the cells regularly maintained at PAR 100 μmol m^{-2} s^{-1} were exposed to HL conditions at PAR 200 μmol m^{-2} s^{-1}, all strains exhibited increased TAG production (*e.g.*, TAG in *Sta*6 increased by a factor of ~3.4). After 72 h, the *Sta*6 showed a factor of ~2.5 increase in TAG levels over the WT that itself grew by a factor of ~2.7. The abundance of TAG for *Sta*1 was on par with its level in the WT strain.

After the light level was reduced from PAR 100 μmol m^{-2} s^{-1} to LL (~0 μmol m^{-2} s^{-1}), the TAG levels in WT and *Sta*1 dropped by a factor of ~1.5 and ~1.3, respectively, whereas for *Sta*6 the TAG production increased by a factor of ~2.8.

Overall, rapid measurements by the LAESI-IMS-MS demonstrated that the *Sta*6 strain under HL conditions was indeed efficiently redirecting energy storage to TAG lipids.

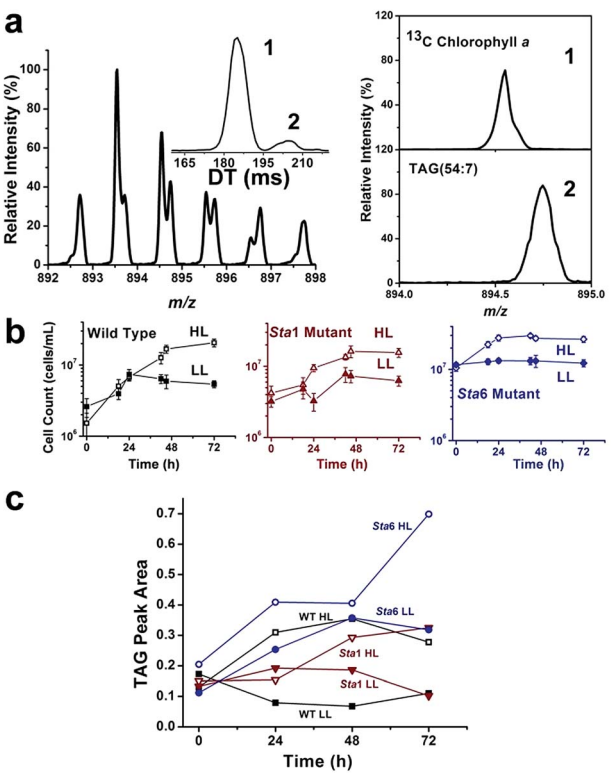

Fig. 7 (a) Interference of ions from two chemical species in the *m*/*z* 892 to 898 range of the mass spectrum (left) of WT *C. reinhardtii*. The inset shows the DT distribution for the nominal *m*/*z* 894 ions. Mass spectra of these ions separated by IMS (right) provides the accurate masses of the two species. (b) Growth rates for WT of *Sta*1, *Sta*6 under HL and LL conditions. (c) Time profile of TAG production by *Sta*1, *Sta*6, and WT *C. reinhardtii* for HL and LL.

Conclusions

Changes in lipid production in the microalga *C. reinhardtii* during light acclimation and due to genetic modifications were followed by LAESI-IMS-MS. This high throughput technique enabled the *in situ* identification of metabolites and lipids from cells in less than 5 min. This compared favourably to the 1 to 2 h required for the extraction and separation (by GC or UHPLC) of lipids using conventional hyphenated MS methods.

Introducing IMS in combination with LAESI compared to LAESI-MS alone increased the number of directly identified TAG species from ~10 to 33. This was, in part, due to the separation of the low TAG signal from the chemical noise in the *m*/*z* region. An additional advantage of the IMS separation compared to UHPLC is the lack of chromatographic overlap between the chemically similar TAG species. This was helpful for the accuracy of relative quantitation of TAG levels under different environmental conditions.

Light conditions were varied between HL and LL and the cellular response was monitored by LAESI-IMS-MS over time in terms of lipid production. In a 72 h period, a significant increase was observed in TAG production (exemplified by the eightfold increase in TAG (50 : 4) levels).

Using LAESI-IMS-MS, we were able to follow the changes in TAG production upon disruption of the starch synthesis. Comparative analysis showed that the most significant increase in TAG production, a factor of ~2.5 over WT, was induced under HL conditions for *Sta*6 mutants. Due to the direct analysis and high throughput capabilities of our method, we were able to demonstrate this in a matter of minutes. As more than 2400 genetically modified *C. reinhardtii* strains are available (http://www.chlamy.org/resources.html, last accessed on July 24, 2014), extensive surveys of their metabolic properties and responses to altered environmental conditions can only be carried out by high throughput analysis methods. The direct analysis protocol described in this paper also ensures minimal perturbation of the metabolism due to the analysis.

Future enhancements of the molecular coverage of this method can be based on utilizing negative ion mode for the LAESI-IMS-MS analysis of molecules with propensity for anion formation (*e.g.*, organic acids), and the application of alternative electrospray solvents. For example, LAESI ion production from molecules of low polarity can be facilitated by electrospray solutions composed of nonpolar solvents.

The developed LAESI-IMS-MS technique can be extended to a wide array of other microorganisms, including bacteria, fungi and viruses. It also readily lends itself to applications in rapid screening of organisms produced by combinatorial genetic engineering.

Acknowledgements

The authors acknowledge financial support from the Chemical Sciences, Geosciences and Biosciences Division, Office of Basic Energy Sciences, Office of Science, U.S. Department of Energy (Grant DE-FG02-01ER15129), a contribution by Protea Biosciences Inc. to the purchase of the Synapt G2S instrument, the

ANR-Biomass-BioEnergies-DiaDomOil grant to support the participation of D.F. in the project and the George Washington University Selective Excellence Fund.

References

1 J. D. Rochaix, *Annu. Rev. Genet.*, 1995, **29**, 209–230.
2 E. H. Harris, *Annu. Rev. Plant Physiol. Plant Mol. Biol.*, 2001, **52**, 363–406.
3 Q.-x. Kong, L. Li, B. Martinez, P. Chen and R. Ruan, *Appl. Biochem. Biotechnol.*, 2010, **160**, 9–18.
4 D. Y. Lee, J. J. Park, D. K. Barupal and O. Fiehn, *Mol. Cell. Proteomics*, 2012, **11**, 973–988.
5 M. C. Davis, O. Fiehn and D. G. Durnford, *Plant, Cell Environ.*, 2013, **36**, 1391–1405.
6 X. Johnson and J. Alric, *Eukaryotic Cell*, 2013, **12**, 776–793.
7 X. Johnson and J. Alric, *J. Biol. Chem.*, 2012, **287**, 26445–26452.
8 D. R. Georgianna and S. P. Mayfield, *Nature*, 2012, **488**, 329–335.
9 R. Miller, G. Wu, R. R. Deshpande, A. Vieler, K. Gaertner, X. Li, E. R. Moellering, S. Zaeuner, A. J. Cornish, B. Liu, B. Bullard, B. B. Sears, M.-H. Kuo, E. L. Hegg, Y. Shachar-Hill, S.-H. Shiu and C. Benning, *Plant Physiol.*, 2010, **154**, 1737–1752.
10 T. S. Moore, Z. R. Du and Z. Chen, *Plant Physiol.*, 2001, **125**, 423–429.
11 C. Giroud, A. Gerber and W. Eichenberger, *Plant Cell Physiol.*, 1988, **29**, 587–595.
12 S.-H. Kim, K.-H. Liu, S.-Y. Lee, S.-J. Hong, B.-K. Cho, H. Lee, C.-G. Lee and H.-K. Choi, *PLoS One*, 2013, **8**, e72415.
13 W. Eichenberger, A. Boschetti and H. P. Michel, *Physiol. Plant.*, 1986, **66**, 589–594.
14 G. A. Thompson, *Biochim. Biophys. Acta, Lipids Lipid Metab.*, 1996, **1302**, 17–45.
15 P. Dormann and C. Benning, *Trends Plant Sci.*, 2002, **7**, 112–118.
16 Z. F. Liu, H. C. Yan, K. B. Wang, T. Y. Kuang, J. P. Zhang, L. L. Gui, X. M. An and W. R. Chang, *Nature*, 2004, **428**, 287–292.
17 I. A. Guschina and J. L. Harwood, *Prog. Lipid Res.*, 2006, **45**, 160–186.
18 M. Siaut, S. Cuine, C. Cagnon, B. Fessler, M. Nguyen, P. Carrier, A. Beyly, F. Beisson, C. Triantaphylides, Y. Li-Beisson and G. Peltier, *BMC Biotechnol.*, 2011, **11**, 7.
19 S. Ball, T. Marianne, L. Dirick, M. Fresnoy, B. Delrue and A. Decq, *Planta*, 1991, **185**, 17–26.
20 R. Ramanan, B. H. Kim, D. H. Cho, S. R. Ko, H. M. Oh and H. S. Kim, *FEBS Lett.*, 2013, **587**, 370–377.
21 V. H. Work, R. Radakovits, R. E. Jinkerson, J. E. Meuser, L. G. Elliott, D. J. Vinyard, L. M. L. Laurens, G. C. Dismukes and M. C. Posewitz, *Eukaryotic Cell*, 2010, **9**, 1251–1261.
22 Z. T. Wang, N. Ullrich, S. Joo, S. Waffenschmidt and U. Goodenough, *Eukaryotic Cell*, 2009, **8**, 1856–1868.
23 Y. Li, D. Han, G. Hu, D. Dauvillee, M. Sommerfeld, S. Ball and Q. Hua, *Metab. Eng.*, 2010, **12**, 387–391.
24 C. Zabawinski, N. Van den Koornhuyse, C. D'Hulst, R. Schlichting, C. Giersch, B. Delrue, J. M. Lacroix, J. Preiss and S. Ball, *J. Bacteriol.*, 2001, **183**, 1069–1077.
25 W. Chen, C. Zhang, L. Song, M. Sommerfeld and Q. Hu, *J. Microbiol. Methods*, 2009, **77**, 41–47.
26 H. Wu, J. V. Volponi, A. E. Oliver, A. N. Parikh, B. A. Simmons and S. Singh, *Proc. Natl. Acad. Sci. U. S. A.*, 2011, **108**, 3809–3814.
27 C. M. Beal, M. E. Webber, R. S. Ruoff and R. E. Hebner, *Biotechnol. Bioeng.*, 2010, **106**, 573–583.
28 V. A. Herrera-Valencia, R. A. Us-Vazquez, F. A. Larque-Saavedra and L. F. Barahona-Perez, *Ann. Microbiol.*, 2012, **62**, 865–870.
29 T. Kind, J. K. Meissen, D. Yang, F. Nocito, A. Vaniya, Y.-S. Cheng, J. S. VanderGheynst and O. Fiehn, *J. Chromatogr. A*, 2012, **1244**, 139–147.
30 J. Jones, S. Manning, M. Montoya, K. Keller and M. Poenie, *J. Am. Oil Chem. Soc.*, 2012, **89**, 1371–1381.
31 K. M. MacDougall, J. McNichol, P. J. McGinn, S. J. B. O'Leary and J. E. Melanson, *Anal. Bioanal. Chem.*, 2011, **401**, 2609–2616.
32 F. Donot, G. Cazals, Z. Gunata, D. Egron, J. Malinge, C. Strub, A. Fontana and S. Schorr-Galindo, *J. Chromatogr. B: Anal. Technol. Biomed. Life Sci.*, 2013, **942**, 98–106.
33 E. Bravi, G. Perretti and L. Montanari, *J. Chromatogr. A*, 2006, **1134**, 210–214.
34 T. Matthew, W. Zhou, J. Rupprecht, L. Lim, S. R. Thomas-Hall, A. Doebbe, O. Kruse, B. Hankamer, U. C. Marx, S. M. Smith and P. M. Schenk, *J. Biol. Chem.*, 2009, **284**, 23415–23425.
35 G. O. James, C. H. Hocart, W. Hillier, H. C. Chen, F. Kordbacheh, G. D. Price and M. A. Djordjevic, *Bioresour. Technol.*, 2011, **102**, 3343–3351.
36 M. Koivusalo, P. Haimi, L. Heikinheimo, R. Kostiainen and P. Somerharju, *J. Lipid Res.*, 2001, **42**, 663–672.
37 M. Schmidt, G. Gessner, L. Matthias, I. Heiland, V. Wagner, M. Kaminski, S. Geimer, N. Eitzinger, T. Reissenweber, O. Voytsekh, M. Fiedler, M. Mittag and G. Kreimer, *Plant Cell*, 2006, **18**, 1908–1930.
38 J. Schiller, J. Arnhold, S. Benard, M. Muller, S. Reichl and K. Arnold, *Anal. Biochem.*, 1999, **267**, 46–56.
39 R. D. Espy, A. Badu-Tawiah and R. G. Cooks, *Curr. Opin. Chem. Biol.*, 2011, **15**, 741–747.
40 M. A. Danielewicz, L. A. Anderson and A. K. Franz, *J. Lipid Res.*, 2011, **52**, 2101–2108.
41 P. Nemes and A. Vertes, *Anal. Chem.*, 2007, **79**, 8098–8106.
42 G. Parsiegla, B. Shrestha, F. Carriere and A. Vertes, *Anal. Chem.*, 2012, **84**, 34–38.
43 G. A. Eiceman, E. V. Krylov, E. G. Nazarov and R. A. Miller, *Anal. Chem.*, 2004, **76**, 4937–4944.
44 R. G. Ewing, D. A. Atkinson, G. A. Eiceman and G. J. Ewing, *Talanta*, 2001, **54**, 515–529.
45 D. J. Weston, R. Bateman, I. D. Wilson, T. R. Wood and C. S. Creaser, *Anal. Chem.*, 2005, **77**, 7572–7580.
46 D. E. Clemmer and M. F. Jarrold, *J. Mass Spectrom.*, 1997, **32**, 577–592.

47 S. D. Pringle, K. Giles, J. L. Wildgoose, J. P. Williams, S. E. Slade, K. Thalassinos, R. H. Bateman, M. T. Bowers and J. H. Scrivens, *Int. J. Mass Spectrom.*, 2007, **261**, 1–12.
48 J. R. McLean, J. A. McLean, Z. Wu, C. Becker, L. M. Perez, C. N. Pace, J. M. Scholtz and D. H. Russell, *J. Phys. Chem. B*, 2010, **114**, 809–816.
49 B. C. Bohrer, S. I. Mererbloom, S. L. Koeniger, A. E. Hilderbrand and D. E. Clemmer, *Annu. Rev. Anal. Chem.*, 2008, **1**, 293–327.
50 B. T. Ruotolo, J. L. P. Benesch, A. M. Sandercock, S.-J. Hyung and C. V. Robinson, *Nat. Protoc.*, 2008, **3**, 1139–1152.
51 P. Dwivedi, G. Puzon, M. Tam, D. Langlais, S. Jackson, K. Kaplan, W. F. Siems, A. J. Schultz, L. Xun, A. Woodsd and H. H. Hill Jr, *J. Mass Spectrom.*, 2010, **45**, 1383–1393.
52 B. Shrestha and A. Vertes, *Anal. Chem.*, 2014, **86**, 4308–4315.
53 M. Kliman, J. C. May and J. A. McLean, *Biochim. Biophys. Acta, Mol. Cell Biol. Lipids*, 2011, **1811**, 935–945.
54 J. Castro-Perez, T. P. Roddy, N. M. M. Nibbering, V. Shah, D. G. McLaren, S. Previs, A. B. Attygalle, K. Herath, Z. Chen, S.-P. Wang, L. Mitnaul, B. K. Hubbard, R. J. Vreeken, D. G. Johns and T. Hankemeier, *J. Am. Soc. Mass Spectrom.*, 2011, **22**, 1552–1567.
55 W. B. Ridenour, M. Kliman, J. A. McLean and R. M. Caprioli, *Anal. Chem.*, 2010, **82**, 1881–1889.

Electronic Supplementary Information for

Metabolic Transformation of Microalgae Due to Light Acclimation and Genetic Modifications Followed by Laser Ablation Electrospray Ionization Mass Spectrometry with Ion Mobility Separation

Sylwia A. Stopka,[1] Bindesh Shrestha,[1] Éric Maréchal,[2] Denis Falconet[2] and Akos Vertes[1]*

[1]Department of Chemistry, W. M. Keck Institute for Proteomics Technology and Applications, The George Washington University, Washington, DC 20052, USA

[2]Laboratoire de Physiologie Cellulaire et Végétale, UMR 5168, CEA-CNRS-INRA-Univ. Grenoble Alpes, Grenoble, France

*Corresponding author: Tel.: +1 (202) 994-2717; fax: +1 (202) 994-5873. E-mail address: vertes@gwu.edu (A. Vertes). Address: Department of Chemistry, The George Washington University, 725 21-st Street, N.W., Washington, DC 20052, USA.

Table S1. Identification of membrane lipids detected in positive ion mode by LAESI-IMS-MS. Identifications were based on accurate mass measurements, isotope distribution patterns, tandem MS, TAP measurements, and database searches. Species marked by * were verified using tandem MS and are represented by their acyl chains in the (sn-1/sn-2) positions.

Identification	Formula	Measured mass *m/z*	Calculated mass *m/z*	Δm (mDa)	DT (ms)
DGTS(32:5)	$C_{42}H_{72}O_7N^+$	702.533	702.5309	2	160.8
DGTS (16:4/16:0)*	$C_{42}H_{74}O_7N^+$	704.547	704.5465	1	159.7
DGTS (16:3/16:0)*	$C_{42}H_{76}O_7N^+$	706.564	706.5622	2	155.0
DGTS (16:2/16:0)*	$C_{42}H_{78}O_7N^+$	708.585	708.5778	7	157.4
DGTS (16:1/16:0)*	$C_{42}H_{80}O_7N^+$	710.597	710.5934	3	159.7
DGTS(32:0)	$C_{42}H_{82}O_7N^+$	712.599	712.6091	10	157.4
DGTS(32:4)	$C_{42}H_{73}O_7NNa^+$	726.533	726.5284	5	155.0
DGTS(16:3/16:0)*	$C_{42}H_{75}O_7NNa^+$	728.546	728.5441	2	155.0
DGTS(32:2)	$C_{42}H_{77}O_7NNa^+$	730.562	730.5598	3	157.4
DGTS(18:4/16:0)*	$C_{44}H_{78}O_7N^+$	732.581	732.5778	4	159.7
DGTS(18:3/16:0)*	$C_{44}H_{80}O_7N^+$	734.591	734.5934	2	163.1
DGTS(34:2)	$C_{44}H_{82}O_7N^+$	736.604	736.6091	5	165.5
DGTS(34:1)	$C_{44}H_{84}O_7N^+$	738.619	738.6248	6	167.8
DGTS(18:3/16:0)*	$C_{44}H_{79}O_7NNa^+$	756.581	756.5753	6	162.0
DGTS(34:2)	$C_{44}H_{81}O_7NNa^+$	758.599	758.5910	9	164.3
DGTS(18:1/16:0)*	$C_{44}H_{83}O_7NNa^+$	760.609	760.6091	0	167.8
DGTS(18:0/16:0)*	$C_{44}H_{85}O_7NNa^+$	762.620	762.6223	2	168.9
MGDG(18:3/16:4)*	$C_{43}H_{68}O_{10}Na^+$	767.474	767.4710	3	152.7
MGDG(34:6)	$C_{43}H_{70}O_{10}Na^+$	769.487	769.4827	4	153.9
MGDG(34:5)	$C_{43}H_{72}O_{10}Na^+$	771.494	771.5023	8	156.2
DGDG(18:3/16:3)*	$C_{49}H_{80}O_{15}Na^+$	931.539	931.5436	4	184.0
DGDG(18:2/16:3)*	$C_{49}H_{82}O_{15}Na^+$	933.557	933.5551	1	187.4
DGDG(18:4/16:0)*	$C_{49}H_{84}O_{15}Na^+$	935.571	935.5707	0	188.6
DGDG(18:3/16:0)*	$C_{49}H_{86}O_{15}Na^+$	937.589	937.5864	2	192.1
DGDG(34:2)	$C_{49}H_{88}O_{15}Na^+$	939.595	939.6021	7	195.5
DGDG (34:1)	$C_{49}H_{90}O_{15}Na^+$	941.616	941.6177	2	196.7

Table S2. Neutral storage lipids detected in positive ion mode by LAESI-IMS-MS. Identifications were based on accurate mass measurements, isotope distribution patterns, tandem MS, TAP measurements, and database searches.

Identification	Formula	Measured mass *m/z*	Calculated mass *m/z*	Δm (mDa)	DT (ms)
TAG(50:5)	$C_{53}H_{92}O_6H^+$	825.699	825.6967	2	184.0
TAG(50:4)	$C_{53}H_{94}O_6H^+$	827.707	827.7123	5	186.3
TAG(50:3)	$C_{53}H_{96}O_6H^+$	829.718	829.7237	6	193.2
TAG(50:2)	$C_{53}H_{98}O_6H^+$	831.732	831.7441	13	197.8
TAG(50:1)	$C_{53}H_{100}O_6H^+$	833.722	833.7297	8	197.8
TAG(50:10)	$C_{53}H_{84}O_6NH_4^+$	834.658	834.6611	3	177.0
TAG(50:0)	$C_{53}H_{102}O_6H^+$	835.774	835.7754	2	178.2
TAG(50:9)	$C_{53}H_{86}O_6NH_4^+$	836.674	836.6768	3	179.3
TAG(50:8)	$C_{53}H_{88}O_6NH_4^+$	838.683	838.6924	9	188.6
TAG(50:7)	$C_{53}H_{90}O_6NH_4^+$	840.707	840.7081	1	190.9
TAG(50:6)	$C_{53}H_{92}O_6NH_4^+$	842.721	842.7238	3	192.1
TAG(50:5)	$C_{53}H_{94}O_6NH_4^+$	844.737	844.7394	3	196.7
TAG(50:4)	$C_{53}H_{96}O_6NH_4^+$	846.755	846.7551	0	199.0
TAG(50:3)	$C_{53}H_{98}O_6NH_4^+$	848.763	848.7708	7	201.3
TAG(50:2)	$C_{53}H_{100}O_6NH_4^+$	850.786	850.7865	0	205.9
TAG(50:1)	$C_{53}H_{102}O_6NH_4^+$	852.786	852.8021	16	205.9
TAG(50:3)	$C_{53}H_{96}O_6Na^+$	851.701	851.7099	9	204.8
TAG(52:8)	$C_{55}H_{90}O_6NH_4^+$	864.701	864.7081	2	193.2
TAG(52:7)	$C_{55}H_{92}O_6NH_4^+$	866.714	866.7238	10	196.7
TAG(52:6)	$C_{55}H_{94}O_6NH_4^+$	868.730	868.7395	9	199.0
TAG(52:5)	$C_{55}H_{96}O_6NH_4^+$	870.751	870.7551	4	200.2
TAG(52:4)	$C_{55}H_{98}O_6NH_4^+$	872.762	872.7708	9	204.8
TAG(52:3)	$C_{55}H_{100}O_6NH_4^+$	874.778	874.7865	9	207.1
TAG(52:2)	$C_{55}H_{102}O_6NH_4^+$	876.790	876.8022	12	208.3
TAG(52:1)	$C_{55}H_{104}O_6NH_4^+$	878.808	878.8179	10	210.6
TAG(54:9)	$C_{57}H_{92}O_6NH_4^+$	890.714	890.7237	10	199.0
TAG(54:8)	$C_{57}H_{94}O_6NH_4^+$	892.734	892.7394	5	200.2
TAG(54:7)	$C_{57}H_{96}O_6NH_4^+$	894.744	894.7550	11	204.8

TAG(54:6)	$C_{57}H_{98}O_6NH_4^+$	896.756	896.7707	15	207.1
TAG(54:5)	$C_{57}H_{100}O_6NH_4^+$	898.769	898.7863	16	208.3
TAG(54:4)	$C_{57}H_{102}O_6NH_4^+$	900.799	900.8020	3	212.9
TAG(54:3)	$C_{57}H_{104}O_6NH_4^+$	902.805	902.8176	13	216.4
TAG(54:2)	$C_{57}H_{106}O_6NH_4^+$	904.826	904.8333	7	216.4

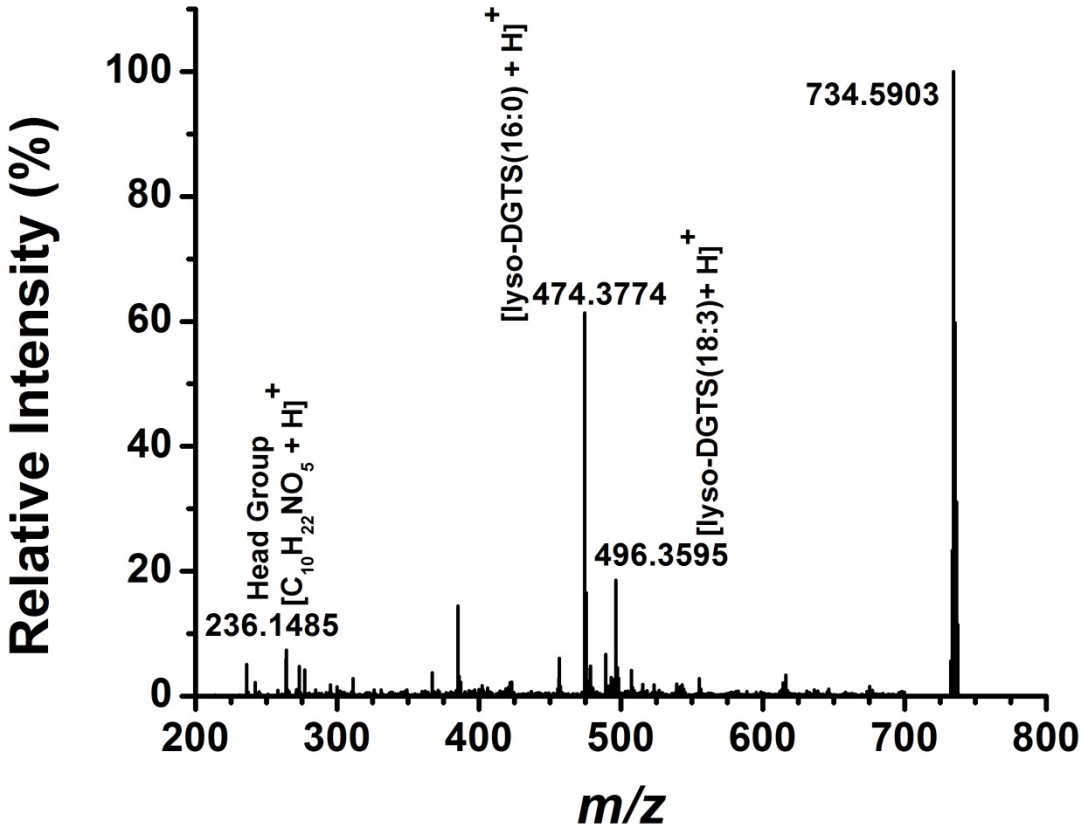

Figure S1. Tandem mass spectrum of protonated DGTS(18:3/16:0) produced by LAESI.

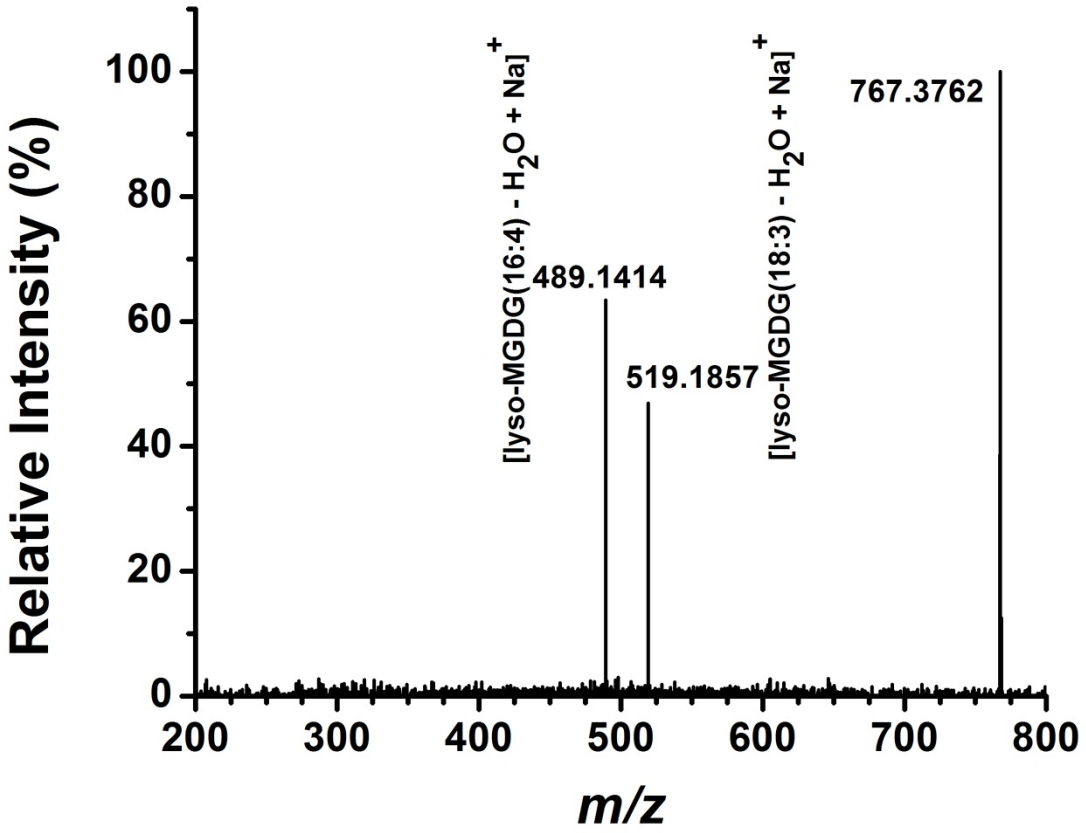

Figure S2. Tandem mass spectrum of sodiated MGDG(18:3/16:4) produced by LAESI.

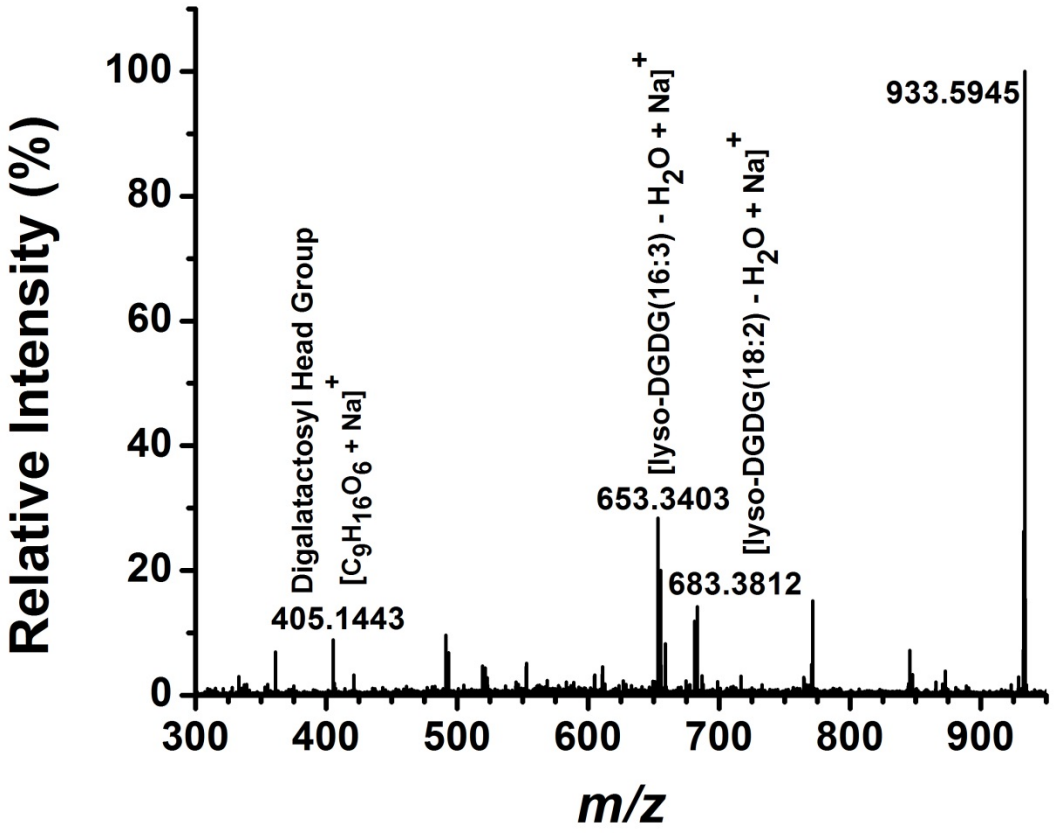

Figure S3. Tandem mass spectrum of sodiated DGDG(18:2/16:3) produced by LAESI.

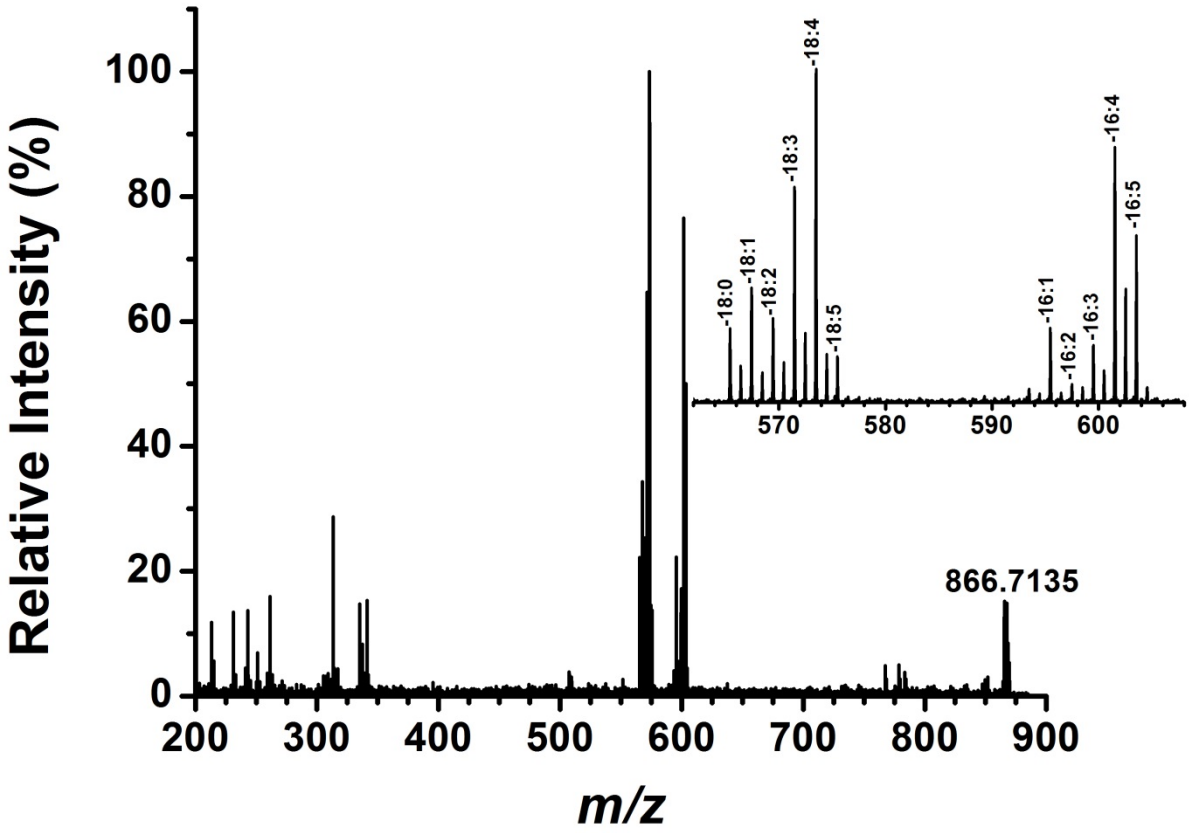

Figure S4. Tandem mass spectrum of cationized TAG(52:7) produced by LAESI-MS. Zoomed version of the fatty acid fragment region is shown in the inset.